Available online at www.sciencedirect.com

SciVerse ScienceDirect

Procedia Engineering 00 (2012) 000–000

Procedia Engineering

www.elsevier.com/locate/procedia

5th BSME International Conference on Thermal Engineering

Towards a transient simulation of Thermo-Acoustic Engines using an electrical analogy

Paul H. Riley [a]

[a]*TheUuniversity of Nottingham, Department of Electrical and Electronic Engineering, Nottingham, NG7 2RD UK.*

Abstract

An electrical analogue of a looped-tube, thermoacoustic engine is presented and simulated using a graphical input, off-the-shelf network analysis tool called Tina™. The analyses are able to show both transient and non-linear behaviour. The recently documented phenomenon from the Score-Stove project of amplitude modulation of the pressure wave, called squegging has been simulated. By use of elements such as Zener diodes to simulate turbulent behaviour, non-linear effects can be seen. Thus the simulation shows the effect of many frequencies, not just the fundamental as is the case with conventional thermoacoustic simulations. Gradual cold start-up, and hot start conditions and a simple technique to ensure mathematical convergence on a non-zero solution are presented.

Keywords: Non-linear; Thermoacoustics; transient-behaviour; Score-Stove; Tina; electrical-analogy; squegging; DeltaEC

Nomenclature

Symbol	Description	Unit	Symbol	Description	Unit
ρ_{tag}	Density of the thermo-acoustic gas at STP	Kg/m3	Tc	Regenerator temperature ambient side	^{o}K
C	Speed of sound	m/s	tc	Regenerator temperature ambient side	^{o}C
C'	Mechanical Volume's Equivalent electrical capacitance b	F	Th	Temperature of the hot side of the regenerator	^{o}K
Dp	Pipe Diameter	mm	th	Temperature of the hot side of the regenerator	^{o}C
L'	Acoustic Inertance's Equivalent electrical	H	v	Particle velocity	m/s
Lp	Pipe length	m	Z0	Characteristic duct impedance, rho x density of the thermo-acoustic gas.	Ns/m
Pa	Atmospheric pressure	Bar	Z0'	Electrical characteristic impedance	Ohms
Pm	Mean pressure in TAE	Bar	τ	Tau, Regenerator thermal time constant	seconds
R'	Equivalent electrical resistancec	Ohms	ω	Frequency	Rads per second
Rp	Pipe loss	Ns/m	ωτ	Regenerator non-dimensional figure of merit	# [1]
Rr	Regenerator loss	Ns/m			
Sc	linear alternator cone area	m2			
Sd	thermo-acoustic duct (pipe) area	m2			

[a] Tel: +44 (0) 115 9515356, email: paul.riley@nottingham.ac.uk

b This is the analogue of a mechanical volume. Note volumes are always connected to ground in the electrical circuit. Series capacitance has no acoustic equivalent.

c Equivalent to mechanical loss

1. Introduction

There are a number of packages currently available for simulating thermo-acoustic engines (TAE), the most well know being DeltaEC [2] written by Swift of Los Alamos laboratories in the US. Most give a reasonably accurate estimation of performance by simulating steady state one dimensional flow. There has also been some success using CFD code[3],[4], analyses using high order differential equations [5] and experimental infrared imaging [6] in predicting non-steady state performance, but setting up the models can be time consuming and difficult to validate. There is much work on electrical analogues in the literature [7] and code already exists to solve the complex mathematics. In real world applications, such as the Score-Stove™ [8], [9] when the heat is produced by a wood flame, understanding of transient behavior would give a result that more closely predicts system performance. Additionally, a transient simulation would enable a better understanding of a phenomenon called squegging [d] [10] [11] [12]. Yu, Jaworski et al [13] have experimentally observed this TAE behavior, but it has not been simulated to our knowledge. Many TAE's generate harmonics that conventional simulations do not model. The electrical analogue has shown some success in predicting this effect as well. This paper presents an electrical analogue of a TAE that uses a commercially available electrical network solver called Tina™ to give transient and steady state behavioral response. The simulation presented can predict qualitively typical transient behavior. Other network solvers can also be used but Tina™ provides an easy to use graphical interface that makes circuit changes both quick to make and more easy to relate to the physical geometry.

2. Circuit Elements

The TAE is modelled using a variety of analogues, described in the following sections. Circuit components have been labelled appropriately to their analogue.

2.1. Mathematical Convergence

Figure 1, Start pulse

Tina™ (version 9.3 and above) will converge with most circuits, and if not, small changes in values can secure convergence. The Resistor models also include a noise element; hence the TAE simulations will sometimes start automatically. However, to ensure operation a starting pulse of 0.1mA for 1ms should be used as shown on Figure 1. This has little effect on accuracy but ensures correct start-up each time.

2.2. Acoustic

Acoustic circuits can be simulated with electrical components in a variety of ways, each with advantages and disadvantages. This electrical analogy of a thermo-acoustic engine uses the following transforms as the author believes that in the Score [9] application they are the most understandable and are shown on Table 1. Table 2 outlines the thermal analogs.

Table 1

Acoustic	**Electrical**
Pressure x Sd	Voltage
Particle Velocity (v)	Current
Acoustic power	V x I
Mass_LA x Sc/Sd	L'
rho * length of pipe /Sd	L'/metre (transmission line inductance)
volume (in m^3) /rho/c^2/Sd^2	C'
Pressure * Sd/Particle velocity	R'

Table 2

Thermal	**Electrical**
Temperature	Voltage
Heat flow	Current
Thermal Mass	Capacitance
Thermal resistance, Rθ	Resistance

[d] Squegging is a term normally used in Electronic RF oscillators to describe unwanted amplitude modulation (AM) of the carrier wave. Similar AM has been seen in TAE's so the term is appropriate to use in TAE applications.

2.3. Sources

There are a number of ways to generate current and voltage. These are called controlled sources. In a TAE, they are used to simulate various parts of a TAE. Figure 2 is a current controlled current source; a velocity amplifier, Figure 3 a voltage controlled current source; pressure to velocity converter, Figure 4 and Figure 5 are more complex controlled sources with the transfer function determined by an equation.

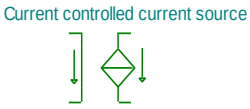

Figure 2, CCCS

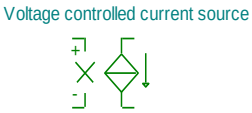

Figure 3, VCCS

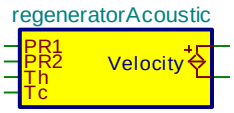

Velocity = (V(PR1)-V(PR2))*((V(Th)+273)/(V(Tc+273)-1)

Figure 4, Four input controlled current source

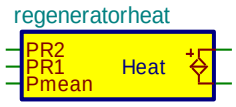

Heat output = (V(PR2)-V(PR1))*(V(PR1)-V(Pmean))*20

Figure 5, three input controlled current source

2.4. Simple Regenerator

The regenerator is effectively a flow modulating device with gain being a function of Th-Tc. In his book [14], Swift models this as a current controlled current source as thermo-acoustically the regenerator is a velocity amplifier. In Tina this is modelled as a voltage controlled current source as this has proven more mathematically stable. The voltage input is scaled by the regenerator loss, to give the equivalent current controlled current source. The circuit is shown on Figure 6 . Regenerator volume is modelled by a capacitance. "Regen loss" is the electrical equivalent of the regenerator flow resistance, and regenerator volume in the total volume of the regenerator itself plus any additional volume associated with the regenerator housing.

The simple model assumes infinite heat flow, so any circuit that uses this method has to limit current flow (particle velocity) by another means. Figure 7 shows Back to back Zener diodes that limit pressure to perform this function. Note the devices chosen should have a very low internal resistance to prevent the current source from forcing the voltage (pressure) to an end stop at infinity. Parallel diodes can also perform this function, but the pressure is limited to 0.7 volts equivalent.

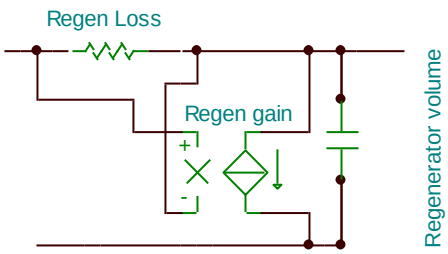

Figure 6, simple regenerator acoustic model

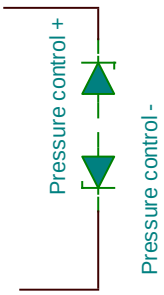

Figure 7, Non-linear pressure control

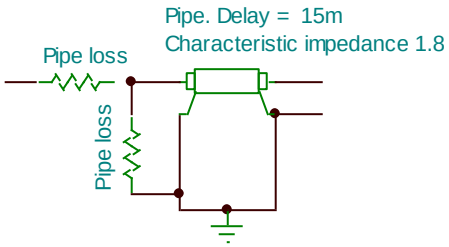

Figure 8, feedback pipe with losses

2.5. Feed back pipes

Pipes are modelled using a lossless transmission line, of characteristic impedance Z0' combined with series and parallel resistors to simulate pipe loss. This method was found to converge more quickly than using the lossy transmission line

component, and it is easier to understand for the non-electrical engineer.

The pipe length is simulated using a delay, where $Delay = \frac{L_p}{c}$ and

Z0 = Characteristic impedance = $cS_d \frac{P_m}{P_a} \rho_{tag}$

2.6. Simple Linear Alternator

Wakeland [15] describes a typical Linear Alternator analogue that can be used in the TAE. Figure 9 describes a simplified model for a loudspeaker working as a linear alternator where the speaker resonant frequency is less than the TAE operating frequency. When operating above resonance, a speaker behaves as an inductance. The resistance represents mechanical and electrical losses as well as load resistance. Power in the resistor therefore represents total acoustic power absorbed.

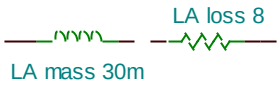

Figure 9, Simple linear alternator model, working above resonance

Figure 10, reference conditions are represented by the ground symbol

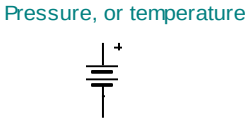

Figure 11, conditions away from reference use a voltage source.

2.7. Measurement

Tina™ allows the operator to place voltmeters (pressure transducers), ammeters (particle velocity) and power meters around the circuit. The transient solver can show start up, steady state operation or cool down characteristics depending on the time chosen for the start and finish of the simulation. Figure 12 shows a voltmeter that reads pressure x duct area. (the equivalent of force). By the addition of an ideal transformer with turns ratio = Sd, Figure 13 shows how to obtain a direct reading of pressure in real units, for example Pascals.

In Figure 14 particle velocity can be read directly. Power is computed (Figure 15) by inserting the horizontal wire into a velocity circuit, and the vertical wire to measure pressure. Reference conditions, for example 0^{O}C, 0 Bar gauge etc. are defined using the ground symbol, Figure 10. Conditions away from reference are modelled using a current source (for velocity and heat flow) or voltage source as shown on Figure 11.

Figure 12, Voltmeter reads pressure x Sd

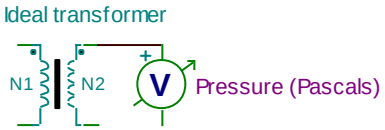

Figure 13, Ideal transformer converts to real units.

Figure 14, An ammeter displays particle velocity in m/s

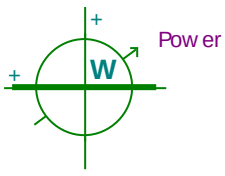

Figure 15, Power measurement.

3. System

The models described below have all been tested using Tina version 9.3 obtainable from here: http://www.designsoftware.com/home/English/& . (Note earlier versions of Tina may not converge mathematically)

3.1. Simple acoustics-only analogue

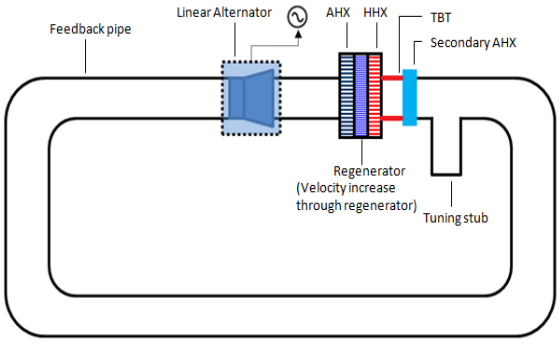

Figure 16 is a diagram of a single regenerator, looped tube TAE and Figure 17 represents the analogue that will self oscillate. Heat flow is excluded from this model. The tuning volume, if short compared with the wavelength can be modelled with a volume (capacitor), Other elements are as described above. A simple resistor models the thermal buffer tube (TBT) and the secondary heat exchanger is not included.

Figure 16, (left) diagram of single regenerator TAE

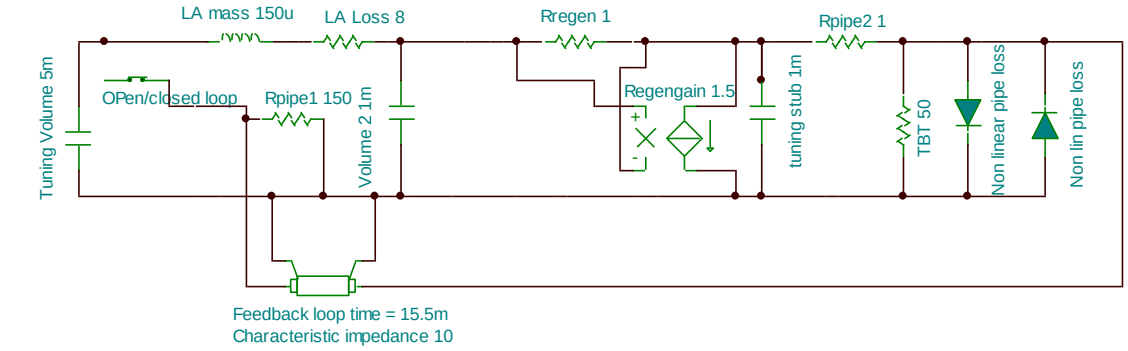

Figure 17, single regenerator TAE analogue

The open/closed switch is used to perform swept frequency measurements to understand open loop system performance to assist in taking the parameters of a non functioning TAE into the oscillating region. This function is outside the scope of this paper and is kept closed in the results described below.

3.2. Single regenerator including thermal

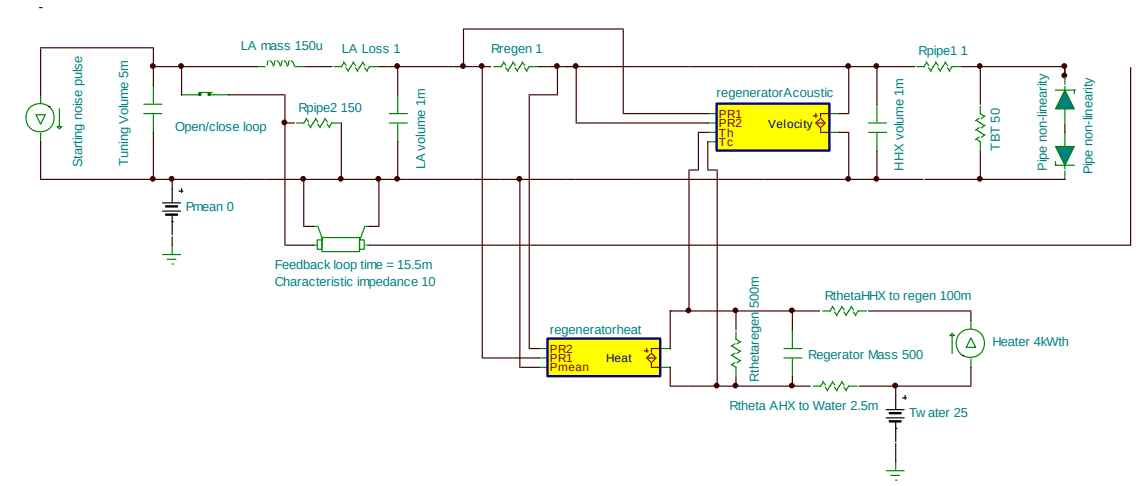

Figure 18, single regenerator TAE including thermal modelling

There are two analogues shown on Figure 18. In the upper section the VCCS of Figure 17 is replaced by the more complex velocity generator that models the acoustic velocity amplification and temperature difference characteristics of a regenerator. The lower section models the thermal characteristic of the regenerator. Ambient temperature is set to 25^{O}C by the voltage source and heat exchanger performance by the thermal resistances and thermal mass (capacitor). A 4 kW constant power heat source is assumed. When oscillation starts, the velocity through regen 1 is multiplied by the pressure to obtain regenerator acoustic power, this multiplied by a constant (effectively the % of Carnot and is empirically derived in this model) then extracts heat from the thermal circuit which, acting in a feedback loop, limits the regenerator temperature.

By adding instrumentation to Figure 18, the important system parameters can be measured. Figure 19 shows the complete circuit used in the simulation results below. These circuits can be found on-line at this reference [16].

Single regenerator with instrumentation

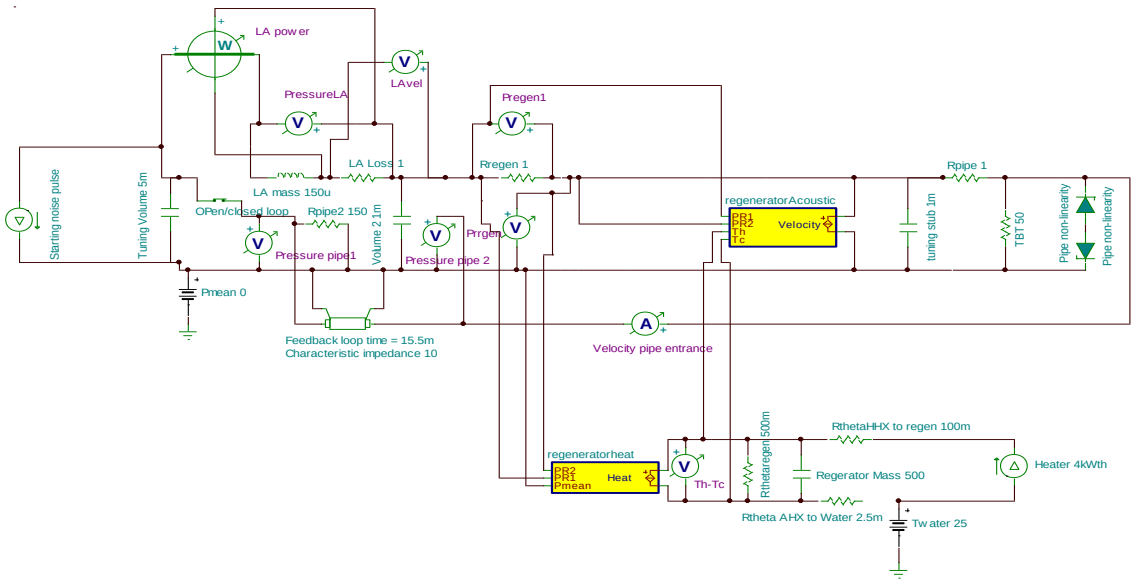

Figure 19, instrumented TAE analogue.

4. Simulation Results

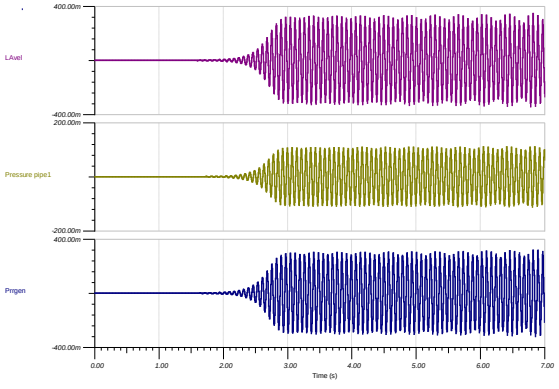

The circuit on Figure 17 produces the start-up shown on

Figure 20. The circuit in Figure 19 produces all the results in subsequent figures. With pipe non-linear loss (the zener diodes) set to a high value (=100), the circuit works in an essentially linear mode and squegging occurs (Figure 23). Lowering pipe non-linear loss to a low value (=15) highlights the effect of large harmonic generation (Figure 24). With normal operation (=50), Figure 21 and Figure 22 show the performance characteristics of typical of a looped tube TAE when started from a hot condition.

Figure 20, normal start-up, acoustic only

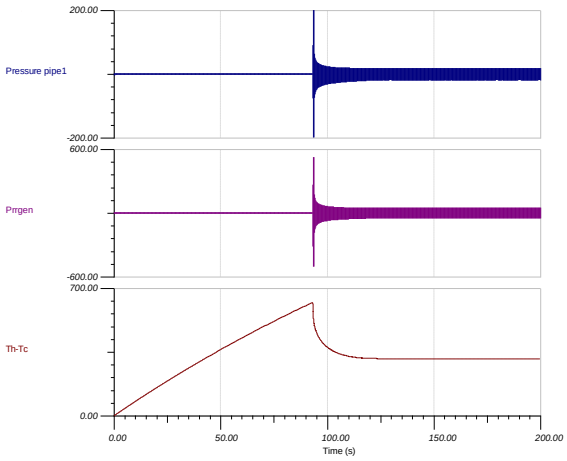

Figure 21, Hot Start up response.

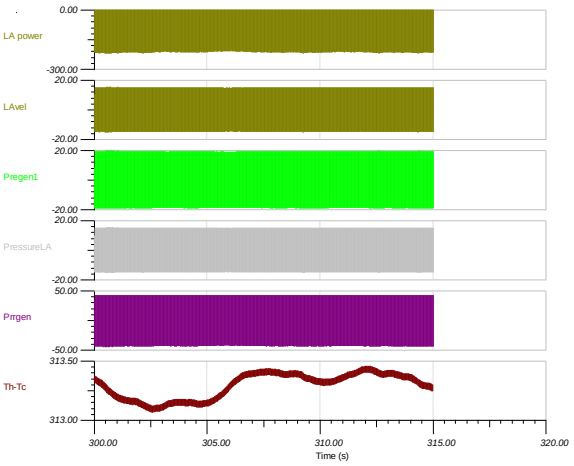

Figure 22, expanded Figure 21 showing ~steady state operation

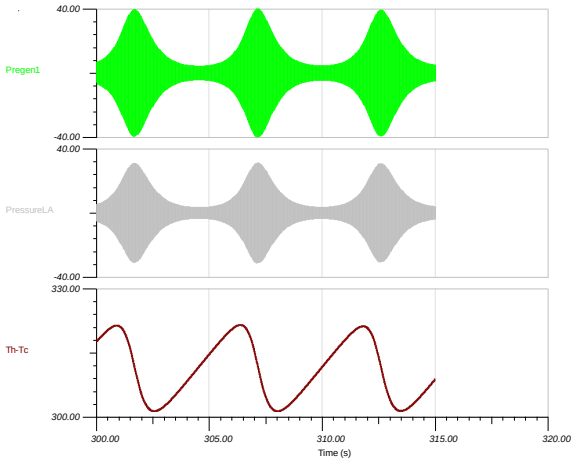

Figure 23, heavy squegging in what should be a steady state condition.

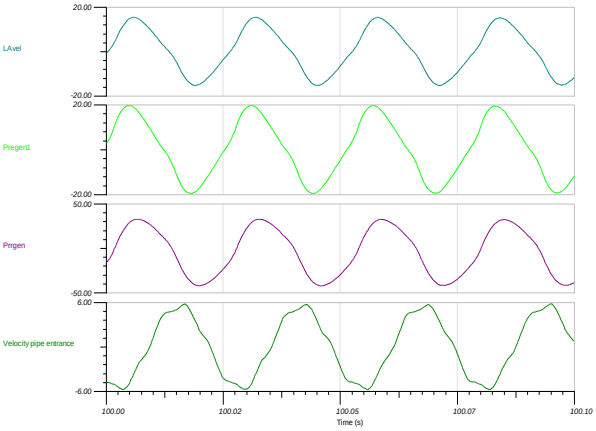

Figure 24, Harmonic generation (non-sinusoidal waveforms)

5. Conclusions

Both transient and pseudo-steady state behaviour of a thermo-acoustic engine has been simulated using an electrical analogue. The circuit exhibits, in a qualitive way the unusual effects of squegging and harmonic generation seen in experimental thermo-acoustic engines but not previously simulated. The circuits are easy to change and the diagrams are easily understood with reference to physical geometry. Most of the circuits described have converged mathematically using Tina™ version 9.3 software. The start-up regime can be contrary, but use of a small staring impulse ensures correct operation.

Future work will look at the minimum physical features required to simulate a working TAE so that experimental results can be quantitively compared with the simulations. The method should enable rapid simulation and analysis of TAE engines including more complex ones of the multi-regenerator variety without the large amount of training normally associated with current TAE simulators.

Acknowledgements

Thanks to EPSRC grant EP/J013986/1, my Score colleagues and special thanks to Scott Backhaus of Los Alamos and Kees deBlok of Aster Thermoakoestische Systemen.

Appendix A.

List of Captions

References

[1] “Low operating temperature integral thermo acoustic devices for solar cooling and waste heat recovery” Acoustics 08, K. De Blok.
[2] http://www.lanl.gov/thermoacoustics/DeltaEC.html
[3] “Simulation of a traveling-wave thermoacoustic engine using computational fluid dynamics”, J.A.L.A. Nijeholt, M.E.H. Tijani, S. Spoelstra. J. Acoust. Soc. Am., 118 (4) (2005), pp. 2265–2270
[4] “Study of nonlinear processes of a large experimental thermoacoustic-Stirling heat engine by using computational fluid dynamics”, G.Y. Yu, E.C. Luo, W. Dai, J.Y. Hu
J. Appl. Phys., 102 (7) (2007) (074901-074901–074901-074907)
[5] “Basic treatment of onset conditions and transient effects in thermoacoustic Stirling engines”, A.T.A.M. de Waele J. Sound. Vib., 325 (4–5) (2009), pp. 974–988
[6] “Visualization observation of onset and damping behaviors in a traveling-wave thermoacoustic engine by infrared imaging” Bo Wang et al., International Journal of Heat and Mass Transfer 54, 5070 (2011)
[7] http://mysite.du.edu/~jcalvert/waves/acoucirc.htm
[8] www.score.uk.com
[9] “Designing a Low-Cost, Electricity Generating Cooking Stove”, Riley, P.H., Saha, C., and Johnson, C.M., Technology and Society Magazine IEEE, summer 2010. Digital Object Identifier 10.1109/MTS.2010.937029, 1932-4529/10/$26.00©2010IEEE.
[10] http://en.wiktionary.org/wiki/squegging
[11] “The technique of Radio Design” (Book chapter 4) Zepler, E. E, Chapman and Hall, London; Wiley and OSns, New York, (1943)
[12]
http://books.google.co.uk/books?id=XiKgKdeBi6cC&pg=PA58&lpg=PA58&dq=squegging+radio+handbook&source=bl&ots=yBIxfWbT87&sig=Mf1yaERVKB51Pv2EBzz2pdI4ajg&hl=en&sa=X&ei=Eni6T4yVFqPG0QXG8ZXoBw&ved=0CF8Q6AEwAg
[13] “Fishbone-like instability in a looped-tube thermoacoustic engine”J. Acoust. Soc. Am. Volume 128, Issue 4, pp. EL188-EL194 (2010); (7 pages) Zhibin Yu, Artur J. Jaworski, and Abdulrahman S. Abduljalil
[14] “Thermoacoustics: A Unifying Perspective for Some Engines and Refrigerators”
Greg W. Swift Acoustical Society of America through the American Institute of Physics, 2002 - 300 pages
[15] “Use of electrodynamic drivers in thermoacoustic refrigerators” J. Acoust. Soc. Am. Volume 107, Issue 2, pp. 827-832 (2000) Ray Scott Wakeland.
[16] http://www.score.uk.com/research/Shared%20Documents/Score_Papers/tinaelectricaanalogues.zip

Available online at www.sciencedirect.com

SciVerse ScienceDirect

Procedia Engineering 00 (2012) 000–000

Procedia Engineering

www.elsevier.com/locate/procedia

5th BSME International Conference on Thermal Engineering

Investigation of a Portable Standing Wave Thermoacoustic Heat Engine

Normah M.G.[a]*, Irfan A.R.[b], Koh K.S.[a], Manet A.[c] and Zaki Ab.M.[b]

[a]*Faculty of Mechanical Engineering, Universiti Teknologi Malaysia (UTM), 81310 Johor*
[b]*School of Manufacturing Engineering, Universiti Malaysia Perlis (UniMAP),02600 Perlis*
[c]Universite de Rennes 1, IUT de Saint Malo, France

Abstract

Increasing the efficiency and effectiveness of energy systems remains as one of the critical issues today with depleting energy resources and increasing energy demand. Utilization of alternative fuels and utilization of waste heat has also become a major research area. This study reports an investigation on a development of a portable thermoacoustic heat engine that converts energy from a combustion process into acoustic power. The prime mover operates with a temperature gradient imposed on a celcor ceramic stack which then induced pressure oscillations. The system consists of a 42-cm long stainless steel alloy 304 tube with a diameter of 50 mm open at one end. A propane torch is used to model a potential heat source from biomass combustion. No hot heat exchanger is required while copper plates are used as the ambient heat exchanger. At 500°C, thermoacoustic effects and pressure oscillations have been observed with a calculated power of 50 W at the stack. The system which operates at atmospheric pressure with air as the working fluid indicates the potential in utilizing the heat produced from biomass combustion that is widely applied in the rural areas.

Keywords: Thermoacoustic heat engine; energy system, biomass combustion, acoustic power

Nomenclature

dB	decibel
L	length of resonator (cm)
T	temperature (°C)
K	type of thermocouple
K	thermal conductivity (W/m.K)
W	Power (watt)
Greek symbols	
μ	dynamic viscosity (Kg/m.s)
c_p	specific heat capacity (kJ/Kg.K)
σ	prandlt number
δ_k	thermal penetration depth (mm)
δ_v	viscous penetration depth (mm)

* Corresponding author. Tel.: +60-7-55-34577; fax: +60-7-55-66159.
E-mail address: normah@fkm.utm.my

Δx	stack length (cm)
ΔT	temperature difference along the stack (°C)

1. Introduction

The increasing demand for energy across the globe today has put a strain on fossil fuels, the main resources of energy. Despite intensive efforts in improving the efficiency and effectiveness of energy systems, energy issues remain the main concern of developed and developing nations. Thermoacoustic technology is a new technology being explored; a temperature gradient induced by acoustics and oscillations induced by a temperature gradient. A thermoacoustic heat engine converts thermal energy into acoustic power while a thermoacoustic refrigerator/heat pump generates acoustic power from an imposed temperature gradient. The working fluid is generally inert gases like Helium or mixtures of Helium and Xenon.

Since the first experiment by Byron Higgins in 1802 on oscillations produced by a hydrogen flame, investigations have been done to study the practical applications of thermoacoustic effects in heat engines and heat pumps/refrigerators. Feldman first reported a 27 W of acoustic power from 600 W of heat source in his Ph.D dissertation [1], with later researchers investigating the theory that could explain the phenomena, possible optimizations and operations of actual systems [2-10]. This study reports the experiments completed on a portable thermoacoustic heat engine that could possibly be utilized with a cook stove to generate power. Past reported works on a similar purpose system have used an electrically heated high temperature source which is manageable [11-13]. This study investigates the actual heat source that could come from a combustion process.

2. Theory

As fluid particles oscillate near a solid boundary, a temperature gradient is set-up in that wall, reaching a steady value as the fluid-solid heat transfer (thermoacoustics) at the ends balanced that of axial conduction within the solid. A low conductivity material is favorable for the stack to reduce the axial conduction. The thermal penetration depth, δ_k, is the distance through which the thermoacoustic effects take place but the viscous penetration depth, δ_v, attenuates the heat loss due to shear stresses. Thus, ideally a fluid with a low Prandtl number, σ, is desired for the working fluid [14],

$$\sigma = \frac{c_p \mu}{K} = \left(\frac{\delta_v}{\delta_k} \right)^2 \qquad (1)$$

where c_p, μ, and K, are the specific heat capacity, viscosity, and conductivity of the fluid respectively. However, air is used in this study as it is easily available for the final use of the system. The stack length, Δx, as recommended by Swift [14] is

$$\Delta x = \frac{L}{10} \qquad (2)$$

with L being the resonator length. Detailed design variables may be obtained in Swift, 2001 [15].

3. Methodology

A schematic of the thermoacoustic heat engine is shown in Fig 1. It is made of a 50-mm diameter stainless steel alloy 304 with a total length of 42 cm filled with air at atmospheric pressure. Although studies have shown that better efficiency has been obtained at high operating pressure (6-10 bars) with Helium or a mixture of the rare gases, this study focused on the practical application within a rural community. The objective is to model a heat source from a combustion process (i.e. biomass) to run a thermoacoustic heat engine generating power for local use. The stack is made from Celcor ceramic with 100 cells/in^2, cut into a diameter of 50 mm, shown in Fig 2a.

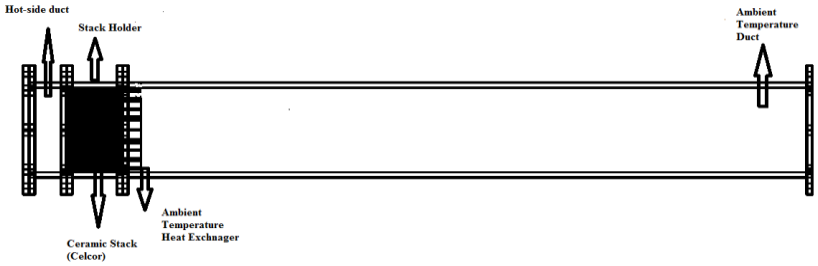

Fig. 1 A schematic of the heat engine.

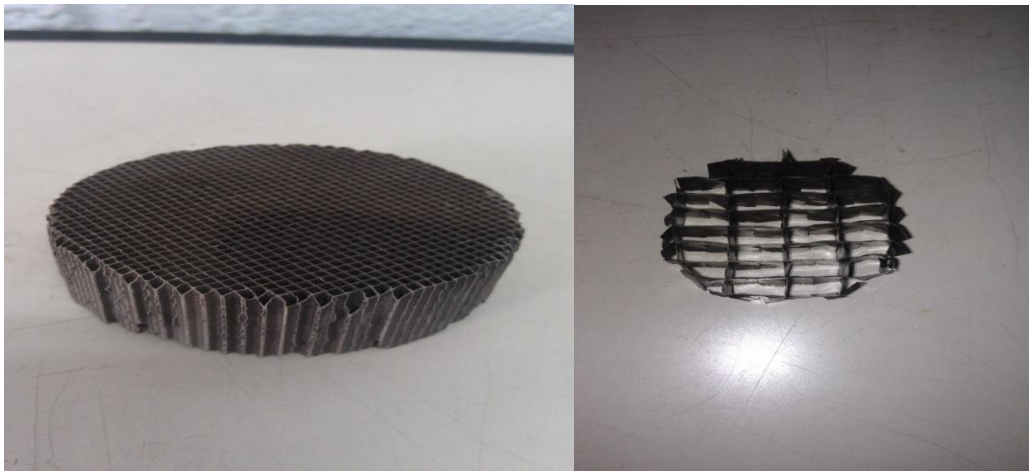

Fig 2. (a) The celcor stack (b) The ambient heat exchanger.

A 2-cm and 3-cm stack length has been studied to look at the acoustics generated from a heat source generated by a propane torch. The source is placed before the opening of the hot-side duct of Fig 1. No hot heat exchanger is used with the heat being directed straight to the stack [13]. The ambient heat exchanger was fabricated from thin copper plates, the dimensions of which are 10 mm by 50 mm with a thickness of 1mm (Fig 2b). The heat exchanger was cut into a 50-mm diameter and positioned next to the Celcor stack within the duct. Four K-type thermocouples are used to measure the temperatures at the mouth of the resonator (T_1), before (T_2) and after the stack (T_3), and the end of the resonator (T_4). A type 26AH microphone amplifier is located at the closed end for measuring the local pressure deviation from the ambient.

4. Results and Discussion

The recorded temperatures over time for the 3-cm stack are listed in Table 1 with the graph presented in Fig 3.

Table 1. Temperature recorded for the 3-cm stack

Time, t (min)	T_1 (°C)	T_2 (°C)	ΔT
0	28.0	28.0	0
5	249.2	40.5	208.7
10	409.0	51.2	357.8
15	468.8	63.5	405.3
20	504.8	66.3	438.5
25	503.0	69.3	433.7
30	511.0	76.5	434.5

A temperature gradient is established along the stack soon after the heat is supplied. This temperature difference induced across the stack indicates that thermoacoustic effects have occurred. The temperature difference for the 3-cm stack seems to stabilize at approximately 20 minutes after the torch was fired, at $\Delta T = 430°C$, which is slightly lower than the maximum temperature difference achieved. Since the celcor ceramic stack in this study was taken from a used catalytic converter of a Proton Perdana V6, a local car, the temperature gradient could have been higher if a new celcor stack had been used. The maximum temperature difference for the 2-cm stack achieved after 10 minutes is 50% lower than that from the 3 cm stack, dropping soon after, shown here in Fig 4. The higher temperature observed at the cold side of the 2-cm stack can be attributed to the axial conduction heat transfer from the hot side thus causing a lower temperature difference across the stack. Although thermoacoustic analysis always assume a short stack approximation such that its presence does not interfere with the acoustic oscillations, an optimum length comparable to the resonator length is required for a stable temperature gradient as seen here.

The pressure measured by the microphone for the 3-cm stack is shown in Figure 5, the increase from ambient fluctuating after 20 minutes. The sound pressure level observed without the background noise is equivalent to 53 dB. Further experiments need to be done to identify if the fluctuating behavior repeats itself to indicate a standing wave profile. No significant sound level was recorded, however, for the 2-cm stack.

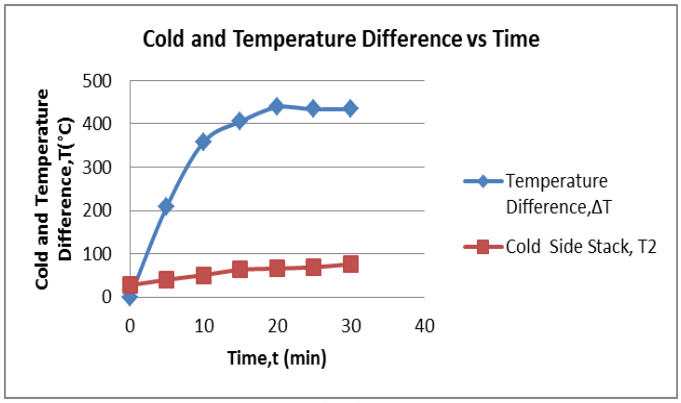

Fig. 3: Temperature profile for the 3-cm stack length

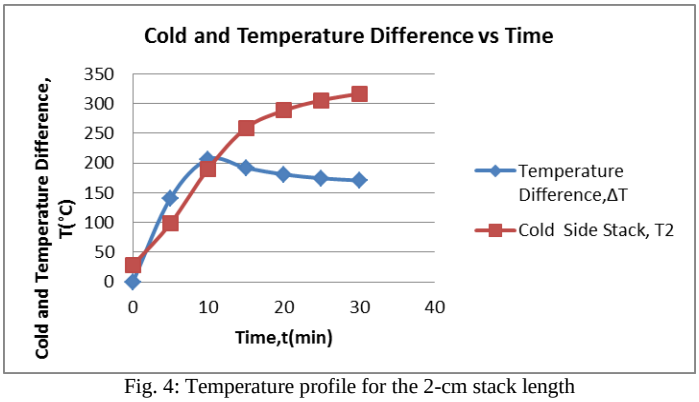

Fig. 4: Temperature profile for the 2-cm stack length

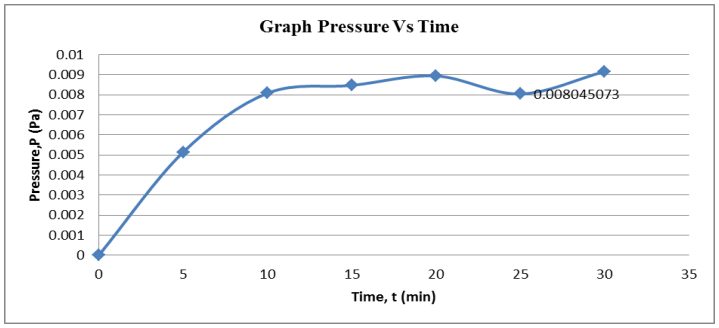

Fig 5 Pressure profile of engine

The overall results from the thermoacoustic heat engine are given in Table 2. The frequency obtained is calculated to be equivalent to a half-wavelength. Although the acoustics obtained may be low, the estimated power generated from the study may be adequate for specific rural household use. The potential application of the thermoacoustic heat engine for remote areas – where biomass combustion in cook stoves is wide spread – can be realized with further studies into the development of the interface between the acoustics generated and power conversion capability. However, the cost of conversion to electricity should be uppermost if the target user is the rural community. Thus, the utilization of waste heat from cook stoves for electricity can be made prevalent.

Table 2. Measured and calculated parameters

Resonator length, L	42.0 cm
Measured parameters:	
Temperature difference across stack, ΔT	433°C
Frequency, f	400Hz
Calculated parameters:	
Acoustic pressure amplitude in the engine,P_A	101kPa
Acoustic power generated in the stack, W	50.67W
Rate of heat supply to the stack, Q_{in}	2952.97W
Thermoacoustic efficiency, $\eta = W/Q_{in}$	1.72%

Conclusion

A portable and simple thermoacoustic heat engine has been developed and results showed the potential application with the heat source possibly coming from biomass combustion. Operating at 1 atmospheric pressure with just air as the working fluid, the low technology prime mover produced up to 50 W of acoustic power at the stack with a heat source at 500°C. Future work should explore the actual heat from a cook stove as well as the interface for power generation at the closed end of the thermoacoustic heat engine.

Acknowledgements

The authors would like to thank Malaysia Ministry of Education FRGS-KETTHA (9003-00352) for supported grand, Universiti Teknologi Malaysia and Universiti Malaysia Perlis for the facilities to do this research.

References

[1] Feldman KT, J of Sound Vib. 1968; 7, 71.
[2] Talom HL and Beyene A, Heat recovery from automotive engine. J. Applied Thermal Engineering 2009; 29:439-444
[3] Nouh MA, Arafa NM, Larsson K and Rahman EA, Design Study of Anharmonic Standing Wave Thermoacoustic Heat Engine. The Sixteenth International Congress on Sound and Vibration 2009; ICSV16, KrakowPoland.
[4] Gardner DL and Howard CQ, Waste heat driven thermoacoustic engine and refrigerator. Proceeding of Acoustic 2009; 23-25, Adelaide Australia.
[5] Stuban N and Torok A, Utilization of exhaust gas thermal energy-theoretical investigation. 33rd Int. Spring on Electronics Technology, IEEE 2010; 268-272
[6] Symko OG and Rodriguez IA, Acoustic Approach to Thermal Management. IEEE Transaction 2010
[7] Kan X, Wu F and Chen L, Constructial of regenerator in a thermo-acoustic engine. Int. J. Of Sustainable Energy 2010; 29: 211-219
[8] Ueda Y and Aoi Y, Critical temperature ratio needed for a spontaneous gas oscillation in a miniature thermoacoustic engine. Proceedings of 20th International Congress on Acoustic, ICA 2010; PACS; 43.35.UD
[9] Wantha C and Assawamartbunlue K, The impact of the resonance tube on performance of a thermoacoustic stack. Frontiers in Heat Transfer (FHMT) 2011; 1-8, ISSN:2151-8629
[10] Liu YW and He YL, Experimental investigation of a thermoacoustic prime mover with helium-argon mixtures as working gas. J. Power and Energy. 2012; 1-9
[11] Symko OG, Acoustic approach to thermal management: Miniature thermoacoustic engines. Transaction IEEE 2006: 0-7803-9524-7/06
[12] Smoker J, Nouh M and Aldraihem O, Energy harvesting from standing wave thermo-acoustic piezoeletric resonator. American Institute of Aeronautical and Astronautics (AIAA) 2010
[13] Montgomery PJ, Low cost thermoacoustic cogenerator for use in biomass burning cook stoves. MSc Thesis 2010, The Pennsylvania State University USA.
[14] Swift GW, Thermoacoustic engine. J. Acosutic Soc. Am.1988; 84:1145-1180
[15] Swift GW, Thermoacoustics: A unifying perspe ctive for some engines and refrigerators. Condensed Matter and Thermal Physics Group Los Alamos National Laboratory 2001

Available online at www.sciencedirect.com

SciVerse ScienceDirect

Procedia Engineering 00 (2012) 000–000

Procedia Engineering

www.elsevier.com/locate/procedia

5th BSME International Conference on Thermal Engineering

CFD investigation of the heat transfer between an external heat source and the regenerator of a thermoacoustic engine

David K. W. Yang[a], Yousif A. Abakr[a*], Normah M. Ghazali[b]

[a]*Department of Mechanical, Manufacturing and Materials Engineering, The University of Nottingham Malaysia Campus, Jalan Broga, 43500 Semenyih, Selangor Darul Ehsan, Malaysia.*

[b]*Faculty of Mechanical Engineering, University Technology Malaysia, 81310 UTM Skudai, Johor Bahru, Malaysia.*

Abstract

The heat transfer between an external source to the regenerator of a thermoacoustic engine involves both convection and radiation heat transfer. In order to enhance the efficiency of the thermoacoustic engine, it is very important to investigate the heat transferred by the two modes to the regenerator. In this paper, the two modes of heat transfer, convection and radiation are under investigation numerically. This work considers the two modes of heat transfer under oscillating flow through the porous medium of the regenerator, the oscillating flow is moving in front of the hot surface of the external heat source resulting in strong convection currents. The CFD modelling and simulation was conducted using Ansys_Fluent™ CFD software. The results show the strong influence of the convection currents and its strong relations to the amplitude and frequency of the vibrations of the oscillating flow. The results also show the importance of radiation heat transfer between the hot surface and the regenerator and the role it may play on the performance of the engine.

Keywords: CFD; Thermoacoustic; Regenerator; Radiation heat transfer; Convection currents

1. Introduction

Waste heat recovery and utilising low grade heat sources for useful work was always an interesting issue to many researchers, this can be done by many systems, and one of them is using a thermoacoustic engine. Thermoacoustic engine is a device to realize the conversion between heat and sound energy. When a compressible fluid is rapidly exposed to a heat flux at a limited part of a solid wall, part of the fluid in the immediate vicinity of the wall expands. This gives rise to a fast increase in the local pressure, and leads to the production of pressure waves, which indicates the change of heat to acoustic power [1]. Advantages of thermoacoustic devices include environmental friendliness, potentially high reliability due to simple structure, no moving parts and reasonable efficiency. The fundamental components of a typical thermoacoustic heat engine include a resonator tube, a regenerator and heat exchangers. The essential components of the investigated waste-heat driven thermoacoustic engine are illustrated schematically in Fig. 1. The bulge acts as a radiant heat exchanger that transfers heat from the external heat source to the regenerator. The overall efficiency of the waste-heat driven thermoacoustic engine depends a lot on the efficiency of the heat transfer process from the external source to the regenerator. The bulge is substituted by a convolution which is believed to have a better heat transfer to the regenerator of the engine. The design of the heat exchanging mechanism of the engine is very complicated and highly challenging.

* Corresponding author. Tel.: +60389248143

E-mail address: yousif.abakr@nottingham.edu.my

It is important to supply most of the heat supply to the engine directly to the regenerator top surface for best performance of the engine. The combined and complex mode of heat transfer from the external source to the engine makes this task extremely difficult to be achieved. This work considers the two modes of heat transfer, convection and radiation, under oscillating flow through the porous medium of the regenerator. A three-dimensional model is proposed and implemented in a computational fluid dynamics (CFD) simulation environment. The simulations are obtained by solving the governing equations using the commercially available Fluent^{TM} Software 6.3 [2]. The most significant advantage of using Fluent^{TM} to model such application is that the innumerable fluid models already implemented by it can be efficiently utilised to predict the coupled heat transfer performance. The model is further examined by developing three additional geometries which have different bulge designs. The geometry of the first model of the bulge is essentially a semi-circular cylinder, facing the flames by its convex side and facing the regenerator of the engine by its concave side. The second design is the convolution, which is a corrugated steel plate in fins like shape. The other two designs were designed based on the first bulge design but segmented into a smaller semi circles. The present paper is an extension of the previous work [3] with the inclusion of the effect of different faces of surface cluster (FSC) used and also some important issues to be taken into consideration in order to maximize the amount of heat transfer to the top layer of the regenerator while minimizing the intrinsic losses. This investigation is one step towards optimization the heat exchanger design and selection for better convolution or bulge design which transports heat from the flames to the regenerator. The overall objective is to investigate the effect of the use of different radiant heat exchangers on the heat transfer efficiency of the external heat source to the regenerator thereby optimise the acoustic power generated. Two different numbers of faces per surface cluster are used in the current study to assess thoroughly the difference.

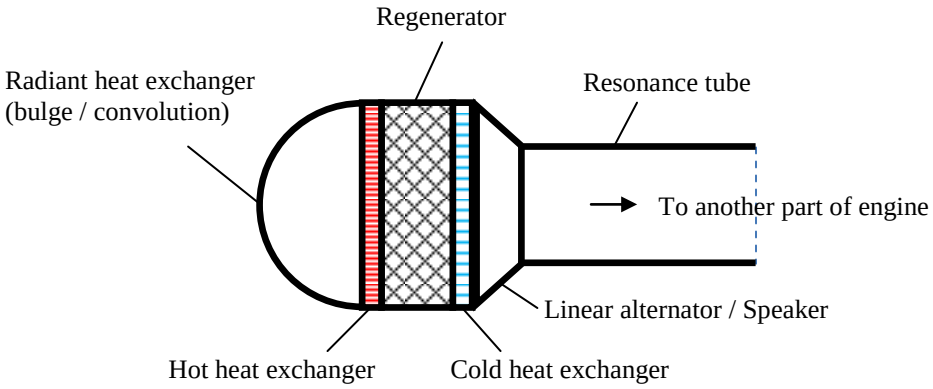

Fig. 1: A section through the basic components of the waste-heat driven thermoacoustic engine.

2. Numerical Approach

There are a total of four different cases; each represents a different geometry in terms of variation of mesh and size. The geometries of the simulation models were first created in the Gambit software. The simulated space consists of mainly two regions; one is the porous zone (regenerator) and the other is the bulge region. The first few layers of the regenerator near the bulge are basically acting as the hot heat exchanger. A 2D schematic one-semicircular cylinder simulation model together with its dimension (in mm) is shown in Fig. 2.

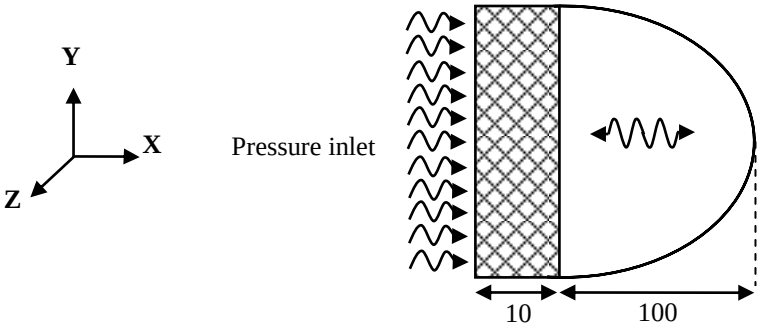

Fig. 2: The XY plane of the schematic one-semicircular cylinder.

All the bulge dimensions are constructed in such a way that all the simulation models possess the same bulge surface areas 0.0628 m^2 except the one-semicircular cylinder bulge model which has the same total bulge volume with the convolution model. The porous region dimensions for all the geometries are the same; each of 200 mm length, 200 mm width and 10 mm thickness. The two surfaces on the z-direction were assumed to be adiabatic wall on one side and an opening on the opposite one. The mesh generated for the geometries are to precisely determine the heat flow of the simulation models. In order to accurately simulate the models, hexahedral mesh is used to mesh the volume of all the four geometries. Meanwhile at the wall, it is made up of quadrilateral meshes which are expected to give better results over a mesh with full triangular grids. Uniform mesh or constant mesh spacing is generated for the geometries. These apply to both the porous and bulge regions. In order to supply a periodic flow for the model, a user defined function (UDF) was developed in C programming language. A harmonic pressure wave Eq. 1 presented was used as an inlet pressure with the aid of user defined function (UDF) in Fluent™.

$$P = P_o + A\sin(v \tag{1}$$

The time average pressure, P_o = 670 Pa was taken as the operating pressure. The coefficient A = 100 Pa is the pressure amplitude; w = 2πf is the angular velocity and f = 80 Hz is the operating frequency of the model. The temperature of the periodic inlet pressure is assumed to have a constant temperature of 674 K. On the other hand, at the bulge surface, the temperature is set to be 1024 K. Constant emissivity, ε of 0.78 and no-slip boundary condition is assigned to all the stainless steel walls. The material properties of stainless steel have density, ρ = 7800 kgm^{-3}, thermal conductivity, k = 21.4 $wm^{-1}K^{-1}$, and specific heat capacity, C_p = 510 $jkg^{-1}K^{-1}$. The most widely used and validated model, standard k-ε model was selected as the turbulence model to account for both the porous media and heat transfer. Thermal effects were also taken into consideration to enhance the heat transfer calculations near the walls. The Reynolds-Averaged Navier Stokes (RANS) equations are used in this work; Fluent™ solves numerically the usual Continuity, Momentum and Energy equations [4, 5]. Fluent solver uses a finite-volume procedure, which converts the governing different equation into algebraic form, together with the SIMPLE (Semi-Implicit-Method for Pressure Linked Equations) algorithm to solve these quantities numerically. For the discretization of the equations the second-order upwind scheme is selected for all the turbulent flow simulations carried out. Surface-to-surface (S2S) model was chosen to model the radiative heat transfer in this study. This model presents a method to obtain the intensity field of radiation exchange in an enclosure of gray-diffuse surfaces. The energy exchange between two surfaces depends on their size, separation distance, and orientation. These parameters are accounted for by the view factors [5]. The main assumption of S2S model is that the exchange of radiative energy between surfaces is unaffected by the medium that separates them. Any absorption, emission or scattering of radiation can be ignored so only "surface-to-surface' radiation needs to be considered for analysis. The S2S model assumes that all surfaces are gray and diffuse. Thus according to the gray body model, if a certain amount of radiant energy (E) is incident on a surface, then a fraction (ρE) is reflected, a fraction (αE) is absorbed, and a fraction (τE) is transmitted. This radiation model also assumes that the heat transfer surfaces are opaque to thermal radiation. The transmissivity, therefore can be neglected. In follows, from the conservation of energy that the emissivity (ε) = absorptivity (α) and that reflectivity (ρ) = 1 - emissivity (ε). The energy flux leaving a given surface is composed of directly emitted and reflected energy. The reflected energy flux is dependent on the incident energy flux from the surroundings, which then can be expressed in terms of the energy flux leaving all other surfaces. Fluent™ uses Eq. 2 for the energy reflected from surface k [6]:

$$q_{out,k} = \epsilon_k \sigma T_k^4 + \rho_k q_{in,k} \tag{2}$$

Where $q_{out,k}$ is the energy flux leaving the surface, ε_k is the emissivity, σ is the Boltzman's constant and $q_{in,k}$ is the energy flux incident on the surface from the surroundings. The amount of incident energy upon a surface from another surface is a direct function of the S2S view factor, F_{jk} . The view factor, F_{jk} is the fraction of energy leaving surface k that is incident on surface j. Eq 3 shows the expression of incident energy flux $q_{in,k}$ in terms of the energy flux leaving all other surfaces [2] :

$$A_k q_{in,k} = \sum_{j=1}^{N} A_j q_{out,j} F_{jk} \tag{3}$$

Where A_k is the area of surface k and F_{jk} is the view factor between surface k and j (N is the number of surfaces). On another form of the aforementioned equation, Fluent™ utilises the radiosity J equation. Eq. 4 shows the total energy given off a surface k [2]:

$$J_k = E_k + \rho_k \sum_{j=1}^{N} F_{kj} J_j \tag{4}$$

Where E_k represents the emissive power of surface k.

To reduce the computational expense, time and storage requirements when a large number of radiating surfaces exist, Fluent™ applies a clustering technique. The number of radiating surfaces is reduced by clustering surfaces into surface "clusters". Two different numbers of faces per surface cluster are use in the current study to assess the difference.

3. Modeling of the Regenerator

The investigated waste-heat driven thermoacoustic engine, the regenerator comprises of 56 layers of stainless steel wire mesh which has a total thickness size of 10 mm. The material properties used for the porous zone is the same as the walls. A volumetric porosity, σ 0.792 is used. The current study uses superficial velocity inside the porous media, based on volumetric flow rate, to ensure continuity of the velocity vectors across the porous media interface. Laminar zone option is disabled so that turbulence effect in porous media will also be taken under consideration. The effect of the porous media on the turbulence field is only approximated. In essence, the porous media is nothing more than an added momentum sink in the governing momentum equations. The porous media is modelled using addition of a momentum source term to the standard fluid flow equations. Eq. 5 shows the source term which composes of two parts; a viscous loss term and an inertia loss term [7]:

$$S_i = -\left(\sum_{j=1}^{3} D_{ij}\mu v_j + \sum_{j=1}^{3} C_{ij}\frac{1}{2}\rho|v|v_j\right) \quad (5)$$

Where S_i is the source term for i the (x, y or z) momentum equation, v_j is the velocity component in j th (x, y or z) direction, |v| is the velocity magnitude and μ is the fluid viscosity. The estimated values for inertial and viscous resistance factors are tabulated in Table 2 as below:

Table 2: Estimated values of inertial and viscous resistance factors.

Data no.	Zone	Average gas particle displacement / mm	Velocity / ms^{-1}	Pressure / Pa	Pressure drop / Pa
1	Porous	2	1.01	447.2	2.36
	Bulge	8	4.02	444.8	-
2	Porous	3	1.52	670.8	4
	Bulge	12	6.03	667.2	-
3	Porous	4	2.02	894.4	4.72
	Bulge	16	8.04	889.6	-
4	Porous	7.1	3.57	1578.3	243.8
	Bulge	24	12.06	1334.5	-
5	Porous	14.2	7.12	3156.6	487.7
	Bulge	48	24.12	2668.9	-

The dependence between the pressure drop, Δp and velocity, v in the porous zone is approximated by means of a second-order polynomial function with the aid of MS Excel using the results tabulated above. Eq.6 is the function found from the graph:

$$\Delta p = 7.43v^2 + 17.4v \quad (6)$$

Eq. 7 shows the momentum equation for the homogenous porous media in a particular direction [8, 9]:

$$\Delta p = C_2\frac{1}{2}\rho\Delta n v_i^2 + \frac{\mu}{\alpha}\Delta n v_i \quad (7)$$

Where α and C_2 are defined as the permeability and the inertial resistance factor of the porous medium respectively. Δn is the porous media thickness and μ denotes the dynamic viscosity. The viscous resistance factor (reciprocal of permeability) and inertia resistance factor can be obtained by comparing Eq. 6 with Eq. 7. For all cases considered in these simulations the convergence criterion or normalised residual for the governing equations is set to be 1e-06. Transient simulations have a fixed time step size of 0.03142 seconds so that 20 time steps will complete a full period of oscillation in the inlet pressure. The maximum iterations per time step is set to be 20 which is sufficient to yield accurate results.

4. Results and Discussion

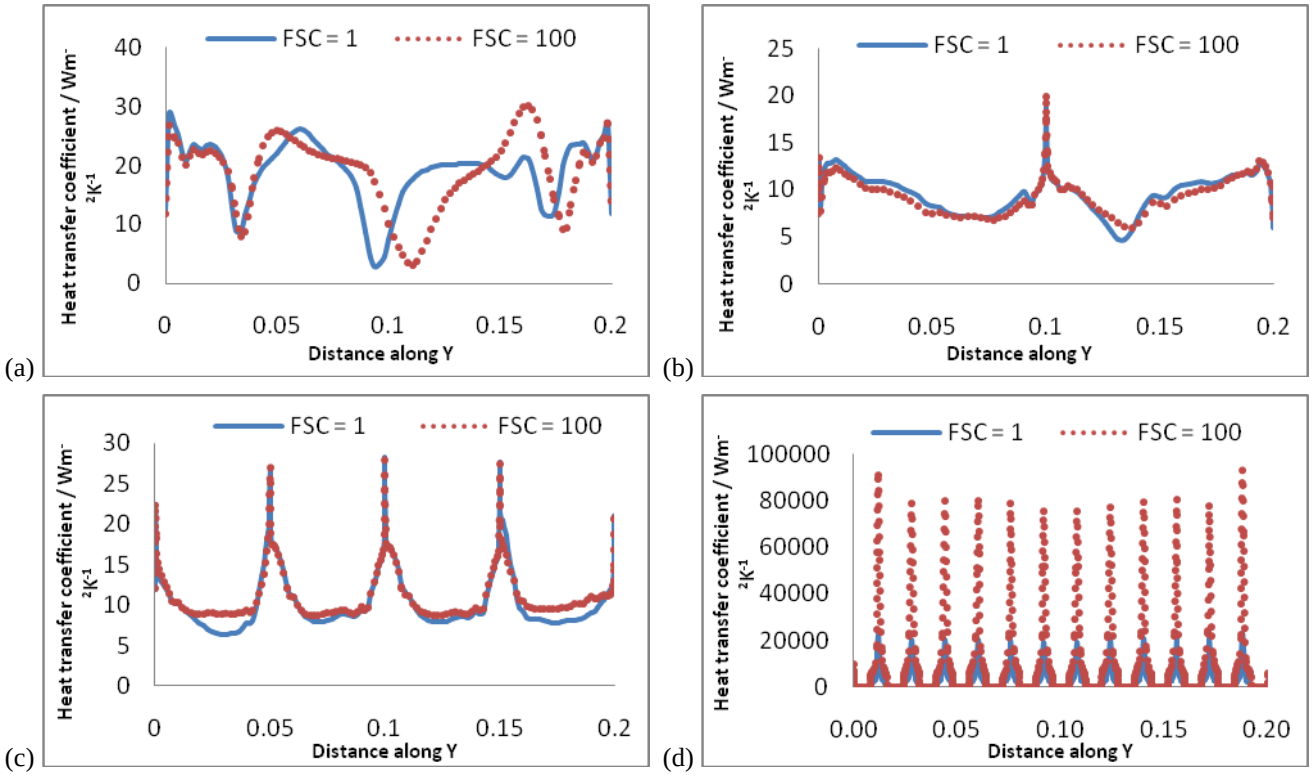

Fig. 3 : The heat transfer coefficient along distance Y for (a) One-concentric cylinder, (b) Two-concentric cylinder, (c) Four-concentric cylinder, and (d) Convolution, at t = 15.7 seconds.

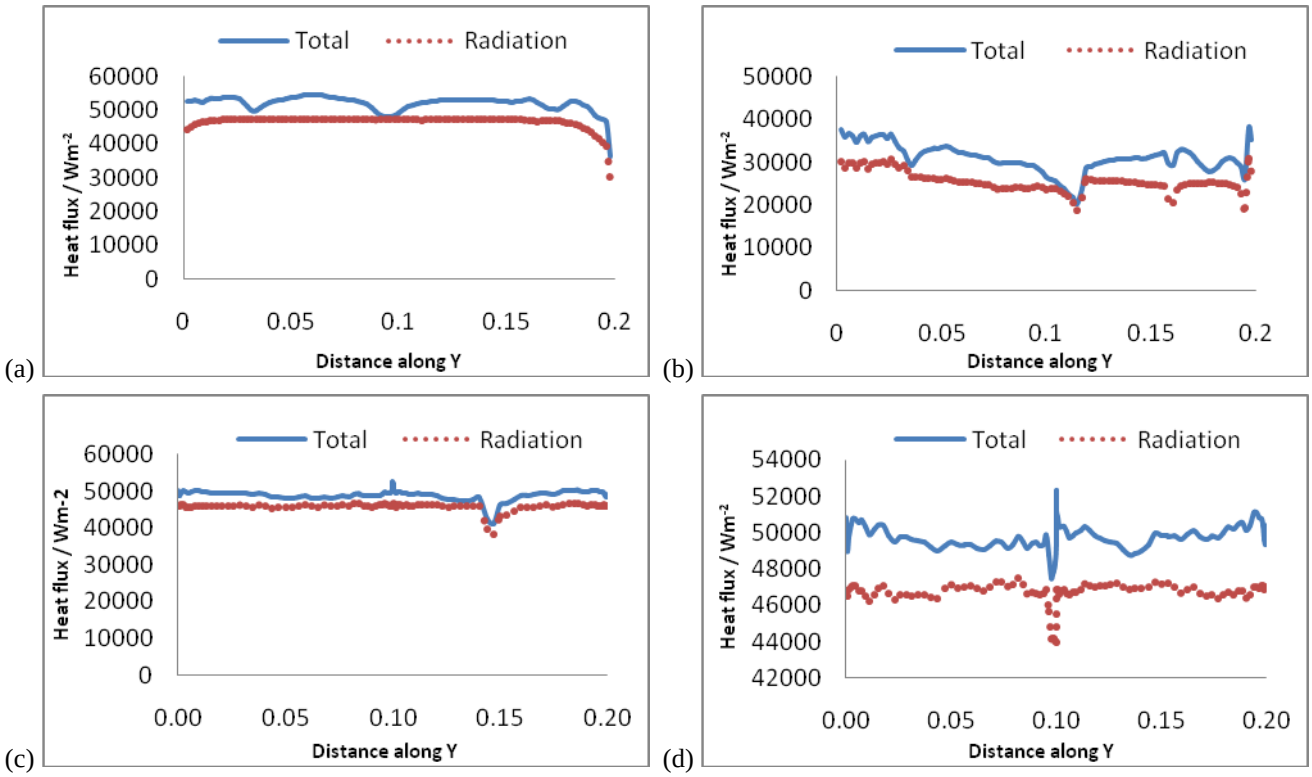

Fig. 4: The total heat flux and radiation heat flux for (a) One-concentric cylinder (FSC=1), (b) One-concentric cylinder (FSC=100), (c) Two-concentric cylinder (FSC=1), and Two-concentric cylinder (FSC=100), at Z = 0.1 m on the bulge/convolution surface at t = 15.7 s.

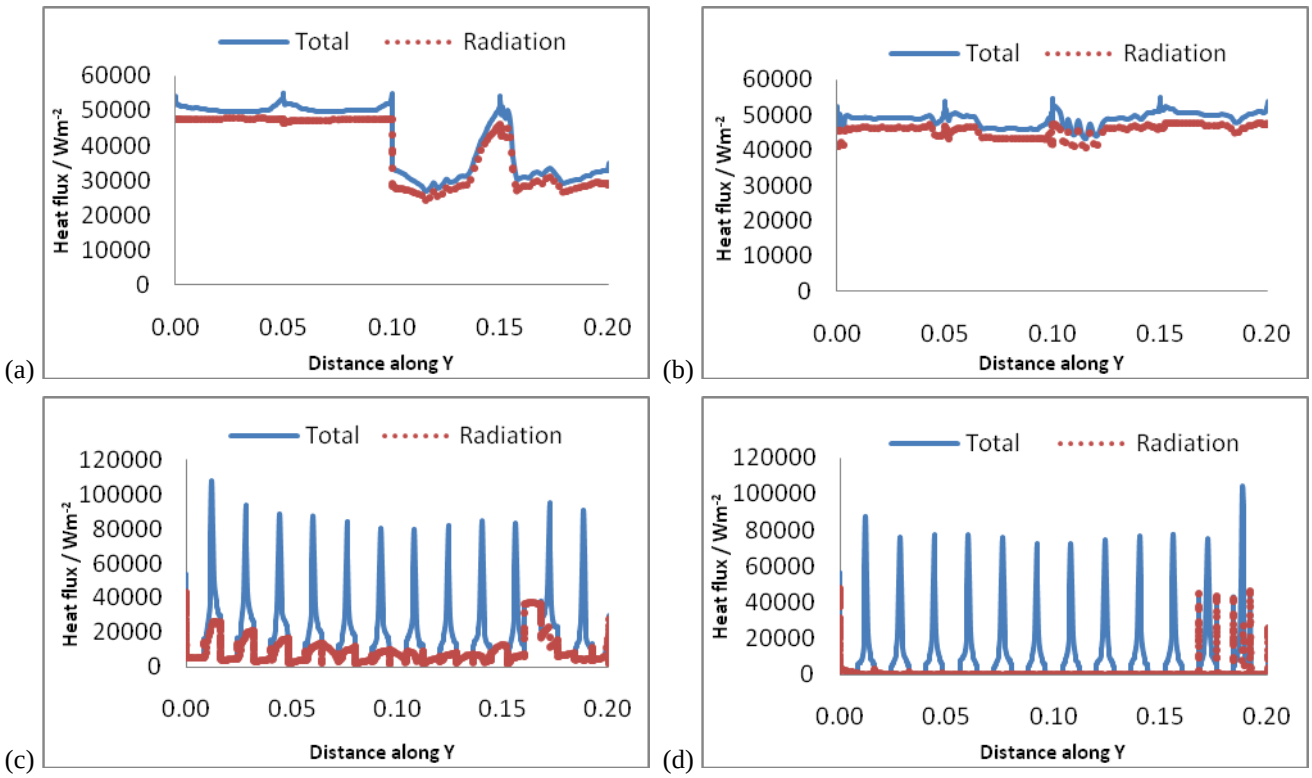

Fig. 5: The total heat flux and radiation heat flux for (a) Four-concentric cylinder (FSC=1), (b) Four-concentric cylinder (FSC=100), (c) Convolution (FSC=1), and (d) Covolution (FSC=100), at Z = 0.1 m on the bulge/convolution surface at t = 15.7 s.

In a waste-heat driven thermoacoustic travelling wave engine, the thermally induced acoustic waves go through a loop rather than recalculating in an enclosed space. The current study had omitted the effect of acoustic waves travelling in a loop. A periodic inlet pressure was used to induce forced convection. The convection prediction is significant, since the design has explicitly tried to reduce the effect of convection. This research study is most concerned about the heat transfer coefficient profile on the bulge surface as it can determine the amount of convection. Fig. 3 presents the relation between the heat transfer coefficient and the distance along the Y direction. The results show a very limited amount of heat transfer by convection. The simulation results indicate variation of faces per surface cluster (FSC) has no significant effect on the trend of the heat transfer coefficient. The two-concentric cylinder exhibits a definite heat transfer coefficient at the centre of Y direction. Approximately 27 $Wm^{-2}K^{-1}$ of heat transfer coefficient is obtained at minimum X vicinity in the bulge region. Owing to the heat flux generated from the adiabatic wall at the partial enclosure temperature, the heat transfer coefficient fluctuates disorderly along the Y direction for one-centric cylinder. Convolution shows a comparatively higher heat transfer coefficient at the minimum X vicinity at the convolution region. This is believed to be caused by the undeveloped turbulence formation near the inlet boundary.

Fig. 4 and Fig. 5 indicate the total surface and radiative heat fluxes along the Y direction. The results in these figures are taken using iso-surface when Z = 0.1 m on the bulge/convolution wall. It can be seen clearly how the total and radiative heat fluxes vary with the distance along Y direction. These figures also show the effect of FSC on the heat fluxes results obtained. All the geometries almost have similar trend regardless of the FSC used. As shown, radiative heat transfer is dominant over the convective heat transfer. The total and radiative heat fluxes appear to be almost uniform along the Y direction when the FSC = 1 for one-concentric cylinder and two-concentric cylinder. A comparatively lower total and radiative heat fluxes are seen at maximum X direction vicinity in the bulge region for one-concentric cylinder and minimum X direction vicinity in the bulge region for two-concentric cylinder when using FSC = 100. Four-concentric cylinder has nearly uniform total and radiative heat fluxes when using FSC = 100. However, when FSC = 1, the total and radiative heat fluxes fluctuate at the Y distance between 0.1 to 0.2. This might be most probably due to the tendency of the adiabatic walls generate heat flux at the partial enclosure temperature. Moreover, it is anticipated that convolution will have a higher total and radiative fluxes at the convolution surface near the porous media. By looking at the heat fluxes solely, one-concentric cylinder and two-concentric cylinder are recommended to improve the engine performance as they both possess high total and radiatiave heat transfer but comparatively lower convective heat flux.

5. Conclusion

Numerical method Fluent CFD modelling with S2S radiation method is used to study the radiation and convection heat transfer in a thermoacoustic engine. This paper presents the results of the study of two modes of heat transfer, to identify the heat transfer characteristic of each one of the two available configurations to improve the design and help on the selection of the ideal shape of the bulge. Based on the results obtained, the design of the bulge will greatly affect the total heat transfer. To accurately predict the heat transfer in the model, conduction must also be included as well. Neglecting conduction heat transfer will result in underestimating the temperature and heat flux which will lead to the miscalculation of total heat flux and etc. There are cases where conduction can be ignored but there are also cases where it must be considered. Future work will answer this question more precisely. The simulations carried out here have shown that some operating parameters and properties can be of high importance in simulations of the heat transfer process dealt with in this paper. In order to investigate the heat transfer in waste-heat driven thermoacoustic engine thoroughly, it is recommended to include the consideration of the gravitational acceleration acting in the outflow direction as the actual design of the engine has thermally induced acoustic flow acting in the outflow direction. Besides that, finer mesh should be created near the bulge wall especially the maximum perpendicular to the regenerator surface direction vicinity to enhance the calculation of heat transfer. In future, the numerical models will be refined through the inclusion of an appropriate atmospheric pressure and by validation with the experimental results.

Acknowledgements

The authors would like to extend thanks to MOSTI funds for funding this work.

References

[1] G. W. Swift, 2002. Thermoacoustic - A Unifying Perspective for some Engines and Refrigerators, Acoustic Society of America
[2] Fluent Inc, 2006. Fluent 6.3 User's Guide.
[3] David Khoo, Yousif A. Abakr, and Normah M. Ghazali, 2012. Numerical investigation on the heat transfer from the cooking stove to the thermoacoustic engine's regenerator, Low-cost, electricity generating heat engines for rural areas.
[4] Bharath M.S, Baljit Singh and P.A.Aswatha Narayana, 2010. Performance Studies of Catalytic Converter Used in Automobile Exhaust System, 37th National & 4th International Conference on Fluid Mechanics.
[5] Adam Neale, Dominique Derome, and Bert Blocken, 2007. Coupled Simulation of Vapor Flow between Air and a Porous Material, ASHRAE.
[6] Imad Qashou, Hooman Vahedi Tafreshi, and Behnam Pourdeyhimi, 2009. An Investigation of the Radiative Heat Transfer through Nonwoven Fibrous Materials, Journal of Engineered Fibers and Fabrics.
[7] Yizhou Ya and Riwan Udin, 2005. Cfd Simulation of a Research Reactor, American Nuclear Conference.
[8] Lukasz Peronski, Roy Bratley, Derek B. Ingham, Lin Ma, Mohamed Pourkashanian, and Stephen Taylor, 2009. Fluid Flow Analysis and Design of a Flow Distributor in a Domestic Gas Boiler Using a Commercial CFD Software, International Journal of Aerospace and Mechanical Engineering.
[9] Y. P. Banjare, R. K. Sahoo, and S. K. Sarangi, 2009. CFD simulation of a Gifford–McMahon type Pulse Tube Refrigerator, International Journal of Thermal Sciences.

Available online at www.sciencedirect.com

SciVerse ScienceDirect

Procedia Engineering 00 (2012) 000–000

Procedia Engineering

www.elsevier.com/locate/procedia

5th BSME International Conference on Thermal Engineering

Experimental investigations on the effects of coiling and bends on the sound energy losses through a resonator tube

David K. W. Yang[a], Yousif A. Abakr[a*], Normah M. Ghazali[b]

[a]*Department of Mechanical, Manufacturing and Materials Engineering, The University of Nottingham Malaysia Campus, Jalan Broga, 43500 Semenyih, Selangor Darul Ehsan, Malaysia.*

[b]*Faculty of Mechanical Engineering, University Technology Malaysia, 81310 UTM Skudai, Johor Bahru, Malaysia.*

Abstract

In order to miniaturize the thermoacoustic engine, thereby to increase their potential applications, coiling the resonator tube is one of the solutions to make it smaller in size (rather than scaling the engine). Whether in a standing wave or travelling wave engine, a resonator is necessary to sustain the driving acoustic waves. However, the curvature of the tube may introduce losses that are not encountered by the normal straight resonator. A straight resonator tube is the easiest design and will have small losses, but it requires large space. However, there are only few studies regarding the effect of resonator coiling. This work investigates the effect of the coiling of the tubes and the bends effects on the efficiency of the sound energy transmission through the tube experimentally. This work consists of the design of an impedance tube system to measure the sound energy losses of coiled tubes of different configurations and comparing the results with the losses in a straight tube. A similar investigation is also conducted for different number of sharp turns of the tubes (u-shaped bend and 90^o bend tube). The impedance tube system designed for the testing consists of an upstream tube, the test section and a downstream tube. The two load method was used to analyze the results by using the four-microphone impedance tube methodology. The results showed significant differences between the four configurations and the outcomes were found to be very useful in the future when designing thermoacoustic looped engine.

Keywords: Thermoacoustic; impedance tube; sound energy losses; resonator tube.

Nomenclature

ρ	density (kg/m^3)
c	speed of sound (m/s)
k	wave number (1/m)
α	transmission coefficient
T_L	transmission loss (dB)
P_n	sound pressure at microphone no. n (Pa)
A_m	the pressure amplitude with respect to Ref axis m for Incident waves
B_m	the pressure amplitude with respect to Ref axis m for Reflected waves
f_L	lower frequency limit (Hz)
f_u	upper frequency limit (Hz)
f_o	fundamental frequency when open end boundary condition (Hz)
f_c	fundamental frequency when closed end boundary condition (Hz)

* Corresponding author. Tel.: +60389248143

E-mail address: yousif.abakr@nottingham.edu.my

s	spacing between two microphones 12 & 34 (m)
l	spacing between the resonator and the closest microphone (m)
X_{ms}	distance between the speaker and the closest microphone (m)
d	inner diameter of the tube (m)
λ	wavelength (m)
L	total length of the impedance tube and the resonator (m)

1. Introduction

Thermoacoustic engine is a device which uses a heat temperature difference to induce high-amplitude sound waves (heat Engine), or uses high amplitude sound waves to pump heat from one place to another (refrigeration). Thermoacoustic engine can be divided in standing wave and travelling wave devices. The typical thermoacoustic device consists of heat exchangers (cold and hot), a resonator, and a stack (on standing wave devices) or regenerator (on travelling wave devices). Depending on the type of engine, a driver or loudspeaker might be used as well to generate sound waves. The resonator in the thermoacoustic engine acts as a pressure vessel (tube) for the working gas that is used to sustain the acoustic wave in the tube. The function of the resonator is to store the acoustic energy to be amplified by the thermoacoustic engine. Besides that, it is also used to transfer the output power of the engine to the acoustic load which could be a heat pump or cooler as well as an alternator [1]. In order to miniaturise the thermoacoustic heat engine, thereby increase their potential applications, coiling the resonator tube is another idea to make it smaller in size. A straight resonator tube is the easiest design and will have a small transmission loss, but it requires large space. The coiling of the resonator will definitely improve the engine footprint but it may introduce losses that are not encountered by the normal straight resonator. The proposed work in coiling the resonator will certainly create more energy losses than the previous designs but the magnitude of these losses are unknown.

There are very few examples in the literature that investigate the energy loss due to resonator geometry. The most important investigation in the energy loss due to resonator geometry is the one carried by Florian et al who investigated the effect of resonator curvature on the thermoacoustic effect using CFD simulation [2]. The variation of pressure amplitude and operating frequency serve as metrics in his investigation. However, no experimental work was carried out as he only focused on the numerical simulation. He showed that the severely curved resonator will exhibit a variation in operating frequency and the amplitude of the acoustic waves. Most importantly, there was no magnitude of energy loss shown in his work.

The overall objective of this work is to investigate the effect of the coiling of the resonators on the efficiency of the sound energy transmission through the resonators thereby optimise the acoustic power transfer between the thermoacoustic engine and the acoustic load (heat pump or cooler). The energy loss (transmission loss) through a Coiled tube was first measured and the results obtained are compared with the energy loss induced in a Straight tube. A similar investigation was conducted for different geometries (U-shaped tube and 90^o bend tube). The impedance tube system designed for the testing consists of an upstream tube, the test section (resonator) and a downstream tube. Tang et al illustrated that the typical lengths used for resonator in thermoacoustic engine is in the range between 4-9 m [3]. Therefore, the lengths for all the resonator geometries were fixed at 4 m long with an inner diameter of 105 mm.

2. Methodology

There are various techniques in the literature used for measuring the sound transmission loss through a test specimen [4, 5, and 6]. The test specimen could be an exhaust system or simply a sound absorbent material in more common. In this work, two-load method developed by Yunseon Ryu & Man-Rim Choi is chosen to calculate the transmission loss through the resonator by using the four-microphone impedance tube technique [7]. Two-load method is the most suitable and easiest method to employ as compared to other existing methods [8, 9].

Instead of moving the sound source from one side to the other, the end boundary condition is obtained by altering the end condition as illustrate in Fig. 1. The removable end cover is adjusted to obtain different boundary conditions. Transmission loss is an important indicator which can effectively determine the how much sound energy is prevented from travelling through the resonator. The transmission loss is found by setting two measurement configurations in order to get two boundary conditions where Eq. 1 and 2 has an open boundary condition at the end of the tube, and Eq. 3 and 4 has the closed boundary condition at the end of the tube:

$$P_1 = A_1 e^{jk(dx1+dx2)} + B_1 e^{-jk(dx1+dx2)} \quad (1)$$

$$P_2 = A_1 e^{jkdx2} + B_1 e^{-jkdx2} \quad (2)$$

$$P_3 = A_2 e^{-jkdx3} + B_2 e^{jkdx3} \quad (3)$$

$$P_4 = A_2 e^{-jk(dx3+dx4)} + B_2 e^{jk(dx3+dx4)} \quad (4)$$

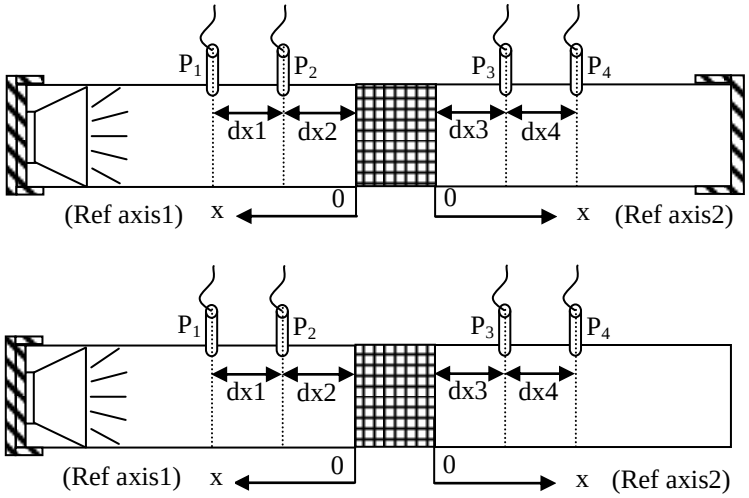

Fig. 1: The schematic diagram of the assembly of the four-microphone impedance tube for both closed and open boundary condition at the end of tube.

In one dimensional wave propagation field, the two pressure waves can be separated into incident and reflected wave respectively. The incident and reflected waves in the upstream tube could be defined as A_1 and B_1 whereas the incident and reflected waves in the downstream tube, passing through the test specimen could be defined as A_2 and B_2.Using the transfer matrix method developed by Yunseon Ryu & Man-Rim Choi [7], the relationship of the pressure amplitude in between the test specimen could be formulated as follow:

$$\begin{Bmatrix} A_1 \\ B_1 \end{Bmatrix} = \begin{bmatrix} \alpha & \beta \\ \gamma & \delta \end{bmatrix} \begin{Bmatrix} A_2 \\ B_2 \end{Bmatrix} \quad (5)$$

$$T_L = 20 \log_{10} |\alpha| \quad (6)$$

3. Impedance tube system

An impedance tube also called as a standing wave tube is an acoustic measurement that provides an effective and easy way for measuring the absorption coefficient and transmission loss of acoustical material. A typical impedance tube consists of microphones, a loudspeaker and sample material. The microphones sense the sound pressure fluctuations and covert them to an analog electrical signal. The loudspeaker acts as a source that generates sinusoidal sound waves which propagate down the tube and reflect from the other end of the tube. The sample material is placed between the tubes to be investigated. In this project, different sample is the tubes with different geometry (Coiled tube, 90^o bend tube, and etc.). In this work, four-microphone impedance tube will be used to evaluate the transmission loss. The impedance tube is designed based on the ISO standard 103534 using the formulas as below [10]:

$$s \ll \frac{0.45}{f_u} c \quad (7)$$

$$l > \frac{d}{2} \quad (8)$$

$$X_{ms} > 3d \quad (9)$$

4. Experimental setup

The impedance tube and resonators have the same circular cross section with an inner diameter of 105 mm. All the tested geometries (resonators) were fixed at 4 m long. These geometries are made from the same material and assumed to have the same surface roughness. The total length of the impedance tube and the resonator is approximately 5 m. The experimental apparatus need to carry out the experiment for the four different geometries are shown clearly on Fig. 2. The sound source used in this work is a loudspeaker which is contained in a transparent sound-insulating box in order to avoid airborne flanking transmission to the microphones. The loudspeaker creates a sinusoidal pressure disturbance that propagates down the tube with the aid of an amplifier. Ring seal socket, a type of o-ring, is used between the impedance tube and the frame of the loudspeaker as well as the loudspeaker box, and also between the impedance tube and the resonator to provide sealing and avoid air leakage. Silicon grid is applied on the surface of the resonator before it is connected to the impedance tube to avoid the socket o-ring to get worn out.

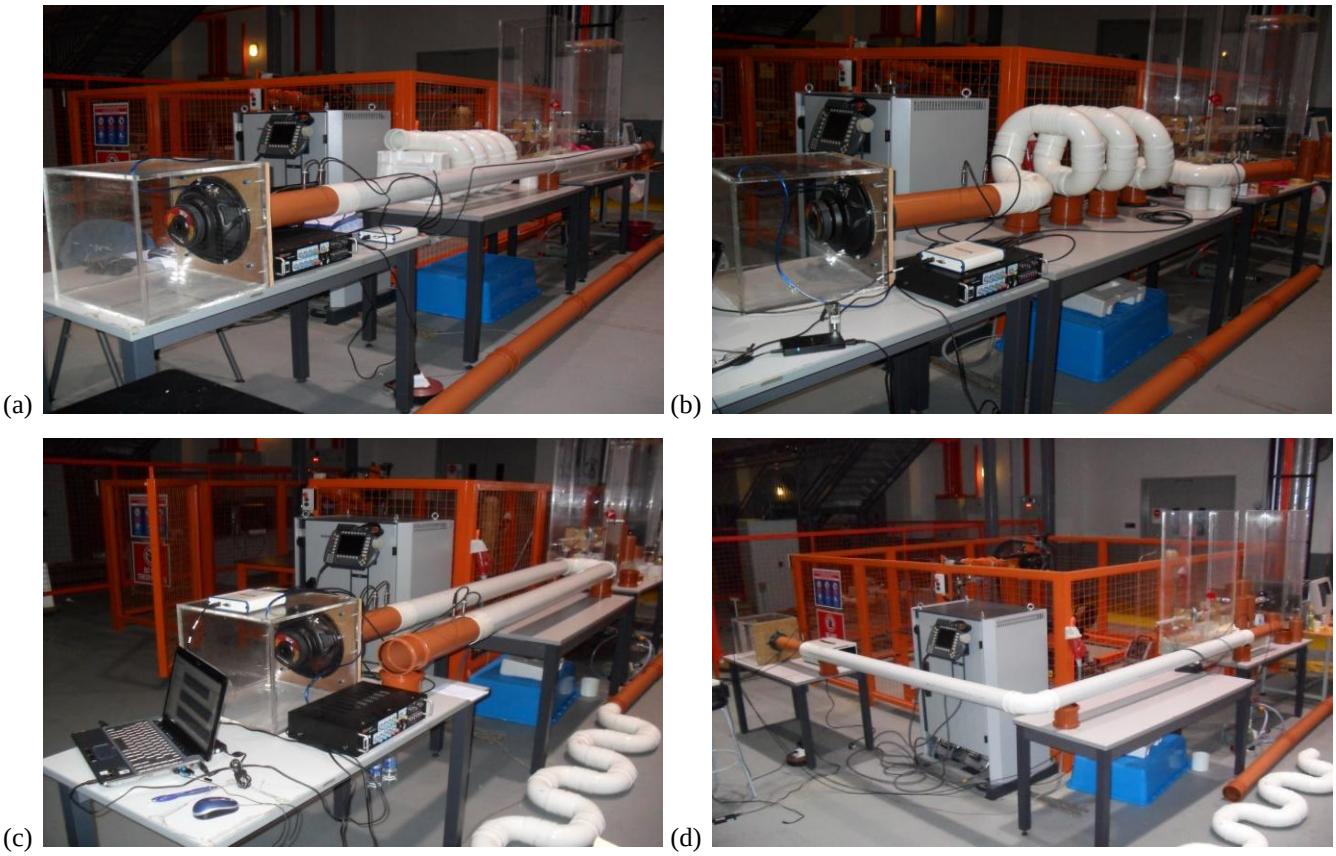

Fig. 2: The experimental apparatus for (a) Straight tube, (b) Coiled tube, (c) U-shaped tube, and. (d) 90^{o} bend tube.

The sound pressure in the tube is collected by the microphones at different locations with the aid of data acquisition. A total of 4 microphones are used to measure the sound pressure along the length of the tube whereby 2 microphones are placed upstream of the tube and the other two are placed downstream. The microphones are sealed tightly to the mounting holes with the aid of rubber and O-ring. All the microphones have a slightly different sensitivity. These microphones are calibrated by using the sound calibrator every time before the experiment is conducted. The measured sound pressure is then used to calculate transmission loss by using both Labview SignalExpress and Matlab. In Labview SignalExpress, the experiment results are collected using filtered and non filtered method. It was found that the non filtered data gives more accurate results. The time-step used in the experiment was 0.001 which means 1000 of data will be collected at 1 second. Maximum pressure was chosen amount the data as the final result to calculate the transmission loss in Matlab.

A signal generator is used to generate a stationary signal with a flat spectral density within the frequency range of interest. The removable end cover is adjusted to obtain open and closed end boundary conditions in the experiment. A standing wave interference pattern results dues to the superposition of the incident and reflected wave. If 100% of the incident wave is reflected, then the incident and reflected waves have the same amplitude; the nodes in the pipe have zero pressure and the antinodes have double the pressure. If some of the incident sound energy is dissipated during the transmission due to the friction loss near the wall for instance, then the incident and reflected waves have different amplitudes; the nodes in the pipe no longer have zero pressure. The pressure amplitudes at the nodes and antinodes are measured with the microphones. The wavelength of the sound emitted by the source (loudspeaker) can be adjusted, but it should be kept substantially larger than the tube diameter, so that plane wave assumption holds. According to the ISO standard 10534-2, the dimensions of the experimental setup determine the working frequency range. The lower frequency limit, f_L depends on the microphone spacing whereas the upper frequency limit, f_u depends on the diameter of the tube [11]:

$$f_u < 0.58 \text{ x } \left(\frac{c}{d}\right) \tag{10}$$

$$f_L < 0.75 \text{ x } \left(\frac{c}{L-d}\right) \tag{11}$$

For the 105 mm inner diameter tube, the working frequency range is 53 Hz < f < 1895 Hz. In order to avoid the occurrence of non-planar wave mode propagation and to assure accurate phase detection, resonance frequencies or overtones are used as the operating frequency for both open and closed boundary conditions. To avoid the phase mismatch between the upstream and downstream of the impedance tube, the overtones of the tubes are used as the operating frequency which is in the range of 206-274 Hz. The overtones or harmonic frequencies are the multiple of the fundamental frequency.

5. Results and Discussion

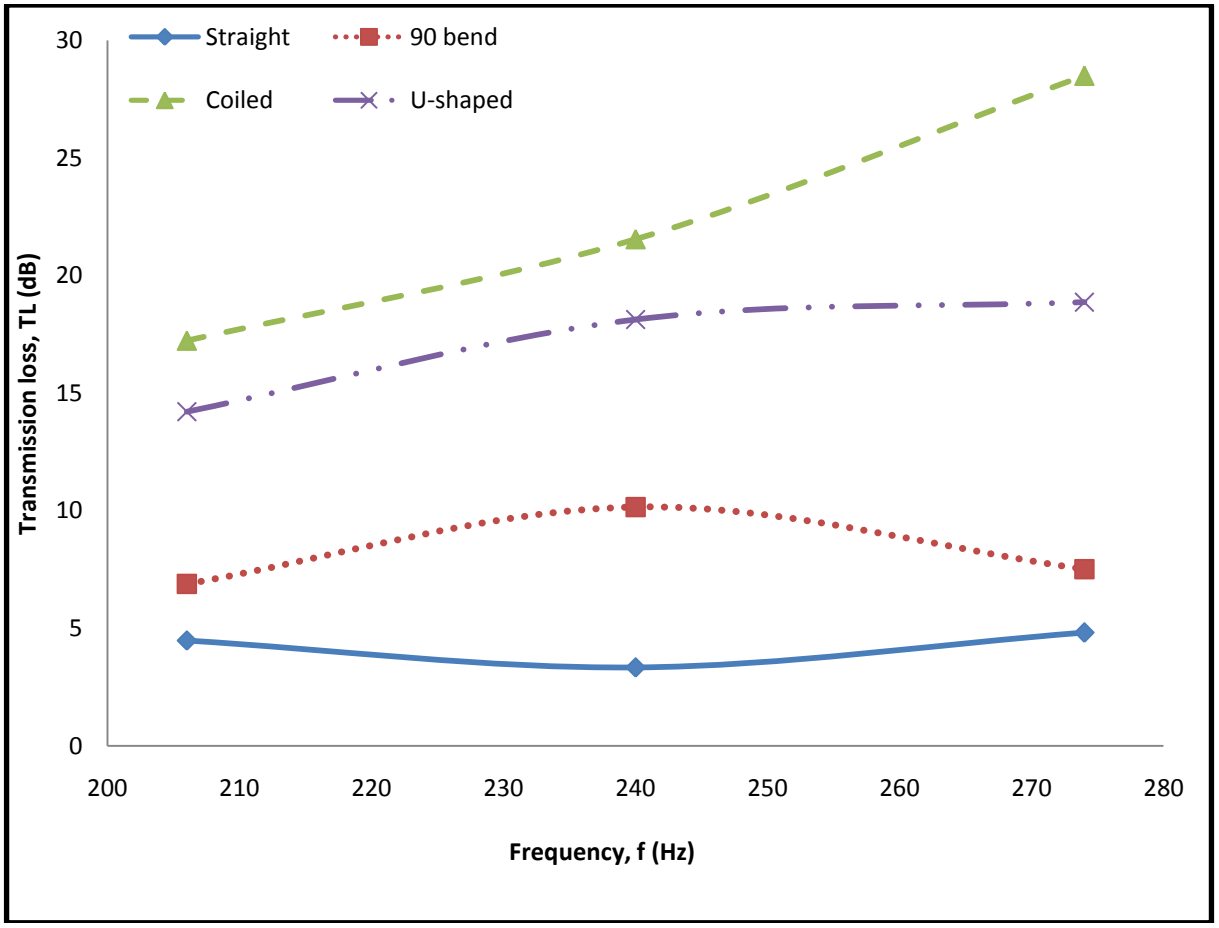

Fig. 3: Transmission loss against frequency for all the four geometries.

As shown in Fig. 3, a general trend can be seen. All the geometries show a gradual increase in transmission loss when the frequency increases except the straight tube and the 90 bends tube. 90^o bend tube gives a higher transmission loss as compared to the Straight tube. Whereas the transmission loss obtained by U-shaped tube is much higher than both Straight tube and 90^o bend tube which is approximately 14 to 19 dB. This can be explained because the U - shaped tube is constructed using two bends and this has led to more losses to be produced. Coiled tube gives the most transmission loss for the all tested frequency as compare to the other three geometries. A very obvious linear transmission loss can be seen as the tested frequency increases. Coiled tube is made up of 16 bends which the number of bends is more than the other three geometries. It is believed that most of the losses came from the air leakage due to imperfect fittings between the resonator and the down and upstream of the impedance tube. The transmission loss obtained for all the four geometries are summarised and presented by a simple flow chart in Fig. 4.

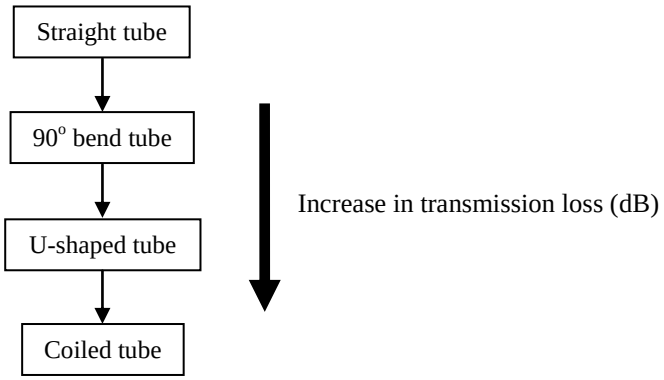

Fig. 4: Flow chart with an order of the increase in transmission loss.

There are a few important factors which lead to the inaccurate results to be collected. Although the microphones were first calibrated every time before the experiment but as time goes by the humidity and temperature in the room changes which turn out the sensitivity of the microphone also changes. Another main factor would be to obtain an exact 4 m long tube for all the geometries. As mentioned earlier in this work, the experiment was conducted using 4 different geometries with the same dimensions. However, the tubes or resonators are not exactly 4 m long as fabricating Coiled tube for instance is not a common product in the market. Therefore, it is made up of several bends instead of one whole tube like the Straight tube. Moreover, another possible error which affects the results taken will be the imperfect sealing between the resonator and the impedance tube. The resonator is connected to the impedance tube by using high force. This high amount of force applied will definitely cause the socket o-ring to get worn out easily although silicon grid was first applied on the surface of the resonator. The quality of socket o-ring will therefore affect inaccurate data to be collected as air leakage will occur. Furthermore, the idea of using overtone as the operating frequency is to avoid inaccurate phase detection. However, the slightly unequalled length of the geometries will cause phase mismatch between the incident and reflected waves in the upstream and also downstream of the tube. Eventually, data are collected at the wrong position which leads to inaccurate results to be collected. In addition, the unwanted sound or noise had propagated into the tube when the open end boundary condition was tested.

The experiment should be carried out in an anechoic room whereby the walls, floor and ceiling are treated with wedge-shaped acoustical absorbing material that absorbs the unwanted sound from surrounding. There is also a certain possibility that unwanted noise was induced when the loudspeaker vibrates and propagates into the downstream section via the tube surface. Instead of placing the loudspeaker directly on the table, a vibration absorber is placed below the loudspeaker to get rid of the vibration. Besides that, it can be seen clearly that the operate overtone would significantly affect the amount of transmission loss through the resonator.

6. Conclusion

The two load method has been used successfully to evaluate the energy loss level in different types of bends and coiled tubes. Based on the experimental results obtained, it can be proven that the Coiled tube gives the most transmission loss, followed by the U-shaped tube, 90^o tube and lastly the Straight tube. The proposed work of Coiled tube will definitely enhance the engine footprint but high transmission loss induced. Straight tube might be the recommendatory geometry as it creates the least amount of transmission loss but requires large space to be stored. Thus, it is suggested that the efficiency of the engine can be further improved by using a smoother one whole tube instead of a making up of several bends. The experiment can be carried out in an anechoic room to avoid unwanted sound in order to predict the results accurately. The future work would be to use DeltaEC, an effective tool used to simulate the thermoacoustic engine, to simulate the energy loss in the resonator.

Acknowledgements

The authors would like to extend special thanks to MOSTI funds for funding this work.

References

[1] S. Spoelstra, J.P. Thermeau, A. J. Jaworski, and C. M. de Blok, 2009. Thermoacoustic Thechnology for Energy Applicatinos, Europan Commission, the Seventh Framework Programme.
[2] Florian Zink, Jeffrey Vipperman, and Laura Schaefer, 2010. CFD simulation of a thermoacoustic engine with coiled resonator, International Communications in Heat and Mass Transfer.
[3] K. Tang, G.B. Chen, T. Jin, R. Bao, B. Kong, and L.M. Qiu, 2005. Influence of resonance tube length on performance of thermoacoustically driven pulse tube refrigerator, Cryogenics.
[4] Mohit Bansal, and Joel Ford, Performance Analysis of Briggs and Stratton Mufflers, 2006. Michigan Tehnological University.
[5] Sung Soo Jung, Yong Tae Kim, and Yong Bong Lee, 2008. Measurement of Sound Transmission Loss by Using Impedance Tubes, Korea Research Institute of Standards and Science.
[6] B. Yousefzadeh, M. Mahjoob, N. Mohammadi and A. Shahsavari, 2008. An experimental study of Sound Transmission Loss measurement technique using impedance tube, Noise Acoustic.
[7] Yunseon Ryu and Man-Rim Choi, 2004. Transmission Loss Measurement of the Exhaust system using 4-Microphones Impedance Tube, Bruel & Kjaer Sound & Vibration Measurement.
[8] Andrew R. Barnard, and Mohan D. Rao, 2004. Measurement of Sound Transmission Loss Using a Modified Four Microphone Impedance Tube, Noise-Con.
[9] Peng Dong-Li, and Hu Peng, 2008. The modified method of measuring the complex transmission coefficient of multilayer acoustical panel in the impedance tube, Applied Acoustic 69.
[10] Yunseon Ryu, 2000. The Acoustic Impedance Measurement System Using Two Microphones, Bruel & Kjaer Sound and Vibration Measurement.
[11] Krishnasudha Vissamraju, 2005. Measurement of Absorption Coefficient of Road Surfaces Using Impedance Tube Method, Osmania University.